Fundamental limits to single-photon detection determined by quantum coherence and backaction

Steve M. Young, Mohan Sarovar, and François Léonard

Phys. Rev. A **97**, 033836 — Published 19 March 2018

DOI: 10.1103/PhysRevA.97.033836

Fundamental Limits to Single-Photon Detection Determined by Quantum Coherence and Backaction

Steve M. Young, Mohan Sarovar, and François Léonard
Sandia National Laboratories, Livermore, CA, 94551, USA

Single-photon detectors have achieved impressive performance, and have led to a number of new scientific discoveries and technological applications. Existing models of photodetectors are semiclassical in that the field-matter interaction is treated perturbatively and time-separated from physical processes in the absorbing matter. An open question is whether a fully quantum detector, whereby the optical field, the optical absorption, and the amplification are considered as one quantum system, could have improved performance. Here we develop a theoretical model of such photodetectors and employ simulations to reveal the critical role played by quantum coherence and amplification backaction in dictating the performance. We show that coherence and backaction lead to tradeoffs between detector metrics, and also determine optimal system designs through control of the quantum-classical interface. Importantly, we establish the design parameters that result in a ideal photodetector with 100% efficiency, no dark counts, and minimal jitter, thus paving the route for next generation detectors.

Modern models of photodetectors and the photodetection process are rooted in pioneering work in quantum optics and quantum electronics [1–5], and have not been significantly modified or updated since. This is surprising given the degree to which experimental photodetection technology has progressed over the past century. Indeed, single-photon photodetectors have been developed based on a wide range of physical processes that span from the photoelectric effect in semiconductors [6, 7] to superconductivity [8–10], and moreover, these photodetectors have achieved impressive performance in terms of efficiency, dark count rate, and jitter [11, 12]. Furthermore, advances in materials science and nanoscale engineering open up possibilities for not only tuning the microscopic properties and dynamics of photodetectors, but also to develop entirely new classes of photodetectors. Such possibilities motivate a re-examination of photodetection theory, with a view on understanding the fundamental limits and tradeoffs. In particular, an open question is whether a photodetector where the electromagnetic field, light-matter interaction and amplification processes are all captured within a single quantum mechanical system could reveal new regimes of photodetector performance. In this work we present such a re-examination of photodetection by developing a fully quantum mechanical minimal model for photodetection and examining the fundamental limits that emerge from this model. Our approach relies on recent advances in quantum optics theory and quantum measurement theory.

The operation of most photodetectors can be viewed as comprising three stages (see Fig. 1): (i) coherent interaction between the electromagnetic (EM) field and a localized system (usually some matter degrees of freedom), (ii) evolution of the state created by the interaction with the EM field according to the internal dynamics of the localized system (this typically tends to localize information about portions of the field state), and (iii) amplification of the information in the internal state(s) of the localized system to classical/macroscopic degrees of freedom.

Typically, it is assumed that the physical processes at each of these stages operate at different timescales, and thus are effectively noninteracting. Such an assumption is implicit in the traditional theory of photodetection and most subsequent treatments that treat the light-matter interaction perturbatively. In this work, we develop a model that makes as few timescale separation assumptions as possible, in order to describe and analyze the photodetection process as an integrated whole. We aim to understand the impact of different internal architectures (*i.e.,* stage (ii)) on the flow of information between the EM field and the amplification process, and, ultimately, the overall performance. This allows us to answer several fundamental design questions, such as: What is the best arrangement of internal states and couplings between them in order to maximize performance? Is a timescale separation between the light-matter interaction and subsequent internal dynamics optimal?

I. MODEL

In order to simulate the dynamics of photodetection we use an open quantum systems formalism [13], and develop a master equation that explicitly accounts for the EM field degrees of freedom, internal degrees of freedom of the detector, and amplification of the detector state to classical degrees of freedom.

We assume that the incoming field contains a single photon with a Gaussian temporal profile $|E(t)|^2 = \left(\frac{1}{2\pi\sigma^2}\right)^{\frac{1}{2}} \mathrm{e}^{-\frac{t^2}{2\sigma^2}}$ of width $\sigma = 1$ns. This field is resonant with an optically active transition in the detector, and couples detector states $|0\rangle$ and $|1\rangle$. To model the response of the detector to this single-photon wavepacket, we utilize the formalism developed in Refs. [14, 15] that treats the field-matter interaction non-perturbatively, which is essential for accurate treatment of detection of such weak field (since the detector dynamics strong modifies the field degrees of freedom in this limit). The cost of this

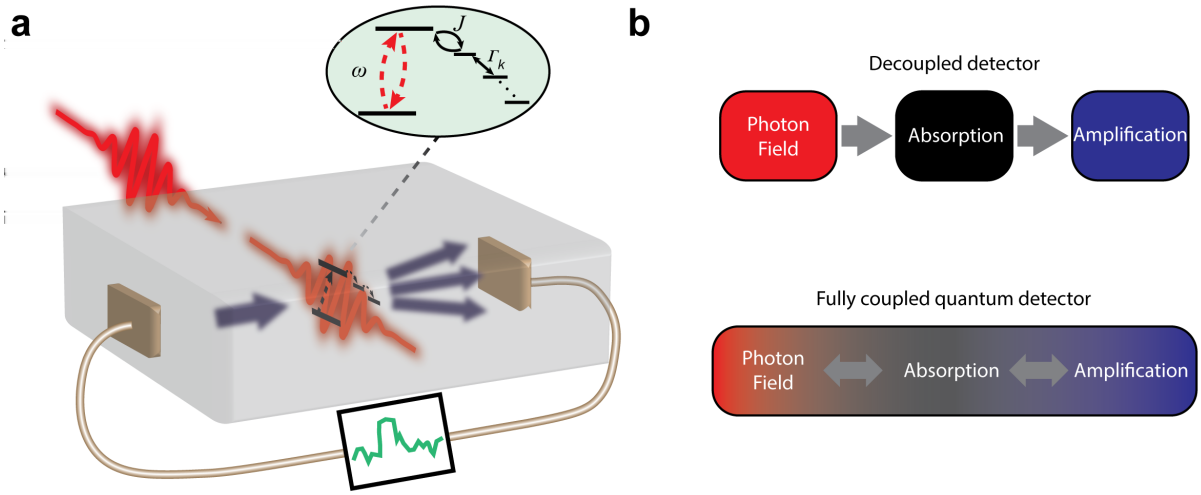

FIG. 1. Single-photon detection in a fully-coupled detector. **a**, Illustration of a photodetector where photon wavepackets interact with the detector (matter) degrees of freedom. The optically coupled excited state can decay into a number of optically inactive states. Information carriers, *e.g.,* electrons, interact with the matter energy levels and scatter, causing a response that can be monitored through a measurement. **b**, The conventional theory of photodetection assumes that the photon field, the absorption process, and the amplification process occur at different timescales and can therefore be treated separately. Alternatively, in this work we consider a fully coupled model where the three subsystems are treated as being part of one quantum system.

non-perturbative treatment is that the evolution equation for the internal state of the detector degrees of freedom, represented by the density matrix $\hat{\varrho}(t)$, involves coupling to an auxiliary (unphysical) matrix, $\hat{\rho}(t)$. The coupled evolution is explicitly, [14, 15]

$$\dot{\hat{\varrho}}(t) = \mathcal{M}\hat{\varrho}(t) + \mathcal{A}\hat{\varrho}(t) + \mathcal{D}[L]\hat{\varrho}(t) + E(t)\left[\hat{\rho}(t), L^\dagger\right] + E^*(t)\left[L, \hat{\rho}^\dagger(t)\right] \quad (1)$$

$$\dot{\hat{\rho}}(t) = \mathcal{M}\hat{\rho}(t) + \mathcal{A}\hat{\rho}(t) + \mathcal{D}[L]\hat{\rho}(t) + E^*(t)\left[L, \hat{\varrho}(0)\right] \quad (2)$$

where $\mathcal{D}$ is the Lindblad superoperator, $\mathcal{D}[X]A \equiv XAX^\dagger - \frac{1}{2}X^\dagger XA - \frac{1}{2}AX^\dagger X$, $\mathcal{M}$ represents the light-independent system dynamics, which may include both unitary and bath-driven evolution, and $\mathcal{A}$ represents the impact of amplification and monitoring. The operator $L = \gamma\,|0\rangle\langle 1|$ represents the field-matter coupling. We assume $\gamma = 1\text{ns}^{-1/2}$, which produces the near-maximal absorption probability of $\approx 80\%$ for an isolated and unmonitored two-state system encountering a pulse of the given width and shape[16]. In order to compare against this base-case, we keep γ fixed at this value for most of the paper (except in Sec. III). In the following we elaborate on the form of the superoperators $\mathcal{M}$ and $\mathcal{A}$..

The optically active internal states of the detector are coupled to a variable number of other states (that are assumed to not interact with the EM field) either coherently or incoherently, see the schematic in Fig. 1(a). These internal states could represent *e.g.,* excitonic or electronic states of a solid-state material, or even electronic or conformational states of molecules. This coupling is captured by $\mathcal{M}$, which describes the dynamics of the internal states that effectively localizes a photoexcitation within the detector degrees of freedom and funnels it away from the optically active state:

$$\mathcal{M}\hat{o}(t) = -i[H, \hat{o}(t)] + \sum_k \mathcal{D}[\Gamma_k\,|e_{i_k}\rangle\langle e_{j_k}|]\hat{o}(t). \quad (3)$$

Here, and in the following, $\hat{o}(t) \in \{\hat{\varrho}(t), \hat{\rho}(t)\}$ since this superoperator appears in Eqs. (1) and (2). H is the Hamiltonian describing the energies of all internal states in the device (denoted $|e_l\rangle$) and coherent couplings between them; Γ_k^2 is the incoherent transition rate from state e_{j_k} to e_{i_k}. Any incoherent transitions are a result of interactions with reservoirs, *e.g.,* phonon degrees of freedom; we do not explicitly model these here, and instead capture their net effect on the essential internal states of the detector.

For the systems under consideration, a designated final internal state, $|X\rangle$, is continuously monitored, a process modeled using a quantum measurement master equation that can be derived from general principles [17–19]. This monitoring effectively amplifies information about occupation of that state by generating a classical measurement record that depends on the population of the state. The average effect of this amplification process is modeled as:

$$\mathcal{A}\hat{o}(t) = \mathcal{D}[\chi\,|X\rangle\langle X|]\hat{o}(t) \quad (4)$$

where χ is the amplification strength. Such a Markovian description of the amplification process is not universal, but importantly, it captures the fact that any amplification process must have an associated backaction on the

system being amplified [20, 21]. In the Appendix we examine a proposed physical device for photodetection and show how one can derive an amplification model like the one used here from the underlying physical interactions.

An advantage to modeling the amplification process as a continuous measurement is that we can utilize quantum trajectory theory [19, 22] to "unravel" a measurement master equation into a stochastic master equation (SME) that enables simulation of individual photodetection records and associated dynamics, in addition to the average dynamics given by Eq. (4). This is achieved by adding to the evolution described by $\mathcal{A}$, the nonlinear term

$$\begin{aligned}&\mathcal{H}[\chi\,|X\rangle\langle X|]\hat{o}(t)\frac{dW(t)}{dt}\\&\equiv\chi\left[|X\rangle\langle X|\,\hat{o}(t)+\hat{o}(t)\,|X\rangle\langle X|-2x(t)\hat{o}(t)\right]\frac{dW(t)}{dt},\end{aligned}\tag{5}$$

where $W(t)$ is a Wiener process [22] and $x(t) = \langle X|\,\hat{\varrho}(t)\,|X\rangle$. Note that this last expectation value, which is what makes this equation nonlinear in the state of the system, is always taken with respect to the physical density matrix $\hat{\varrho}(t)$, even when $\hat{o}(t) = \hat{\rho}(t)$.

The associated measurement current, which this stochastic evolution is conditioned on, is given by

$$I_t = \int_{t-t_m}^{t} \chi^2 \varrho_{XX}(t')dt' + \chi dW(t').$$

where t_m is the integration time window, and $\varrho_{XX}(t)$ is the population of the X state given by the physical density matrix for the detector internal degrees of freedom, $\hat{\varrho}(t)$. In our calculations, we chose t_m values that result in optimal performance for a given χ.

In the following, we numerically integrate the above dynamical equations using the order (2.0,1.5) stochastic Runge-Kutta algorithm proposed in Ref. [23].

II. TWO INTERNAL CONFIGURATIONS

In this section we study two possible configurations for the detector's internal degrees of freedom. Configuration 1, with the final monitored state, $|X\rangle$, being the same as the optically active state $|1\rangle$ (Fig. 2(a)), and Configuration 2, with $|X\rangle$ being a long-lived dark state, $|C\rangle$, to which the optically active state incoherently decays (Fig. 2(b)). In the latter configuration we assume that $|1\rangle$ and $|C\rangle$ are sufficiently separated in energy so that thermally excited population transfer from $|C\rangle$ to $|1\rangle$ can be neglected. Such a thermal effect can be modeled but would only yield a trivial decrease in efficiency of this configuration. In the following, we study both of these configurations using the dynamical model described above and quantify detector performance in terms of efficiency, dark count rates, and jitter.

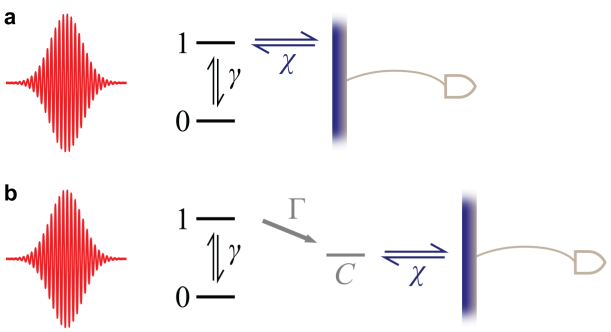

FIG. 2. The two configurations under consideration. In both cases, we consider a single-photon Gaussian wavepacket (left) incident on a two-level system, creating a resonant excitation. A quantum measurement element (vertical purple line) couples to the internal states and amplifies the signal to the classical domain (right). In **a**, the quantum measurement element directly couples to the excited state and so $|X\rangle \to |1\rangle$, while in **b**, the population in the excited state may decay into a third, optically inert state to which the quantum measurement element is coupled, and so $|X\rangle \to |C\rangle$.

A. Configuration 1

For configuration 1, the dynamical equations, Eqs. (1), can be written in component form as

$$\begin{aligned}\dot{\rho}_{01} &= -i\omega_{01}\rho_{01} - \gamma E(t) - \frac{\gamma^2+\chi^2}{2}\rho_{01}; \quad \rho(0) = 0,\\ \dot{\varrho}_{00} &= 2\gamma E(t)\rho_{01} + \gamma^2\varrho_{11}; \quad \varrho_{00}(0) = 1,\\ \dot{\varrho}_{11} &= -2\gamma E(t)\rho_{01} - \gamma^2\varrho_{11}; \quad \varrho_{11}(0) = 0,\end{aligned}$$

with all other elements zero throughout.

The generation of the coherence between states $|0\rangle$ and $|1\rangle$ is damped by both the spontaneous emission back into the photon mode and decoherence due to backaction from the amplification of $|1\rangle$; this restricts the development of the excited state population. Solving the equations for different values of χ makes this concrete; stronger amplification noticeably reduces the excitation probability (Fig. 3a), a manifestation of the Zeno effect [24, 25].

Simulating individual trajectories reveals additional aspects of the tradeoff between information gain and disturbance. Figure 3b shows the excitation population and associated detector output for sample trajectories. For weak amplification, Fig. 3b, the individual trajectories are similar to the averaged case. Unfortunately, due to the weak coupling the current cannot be readily distinguished from the background noise. Stronger amplification significantly alters population evolution and produces trajectories that either completely miss or completely absorb the photon. In this case the current unambiguously distinguishes photon absorption events, but at the price of reduced efficiency due to significant perturbation of the absorption probability.

A more complete picture of impact on photodetection performance emerges after compiling the results over

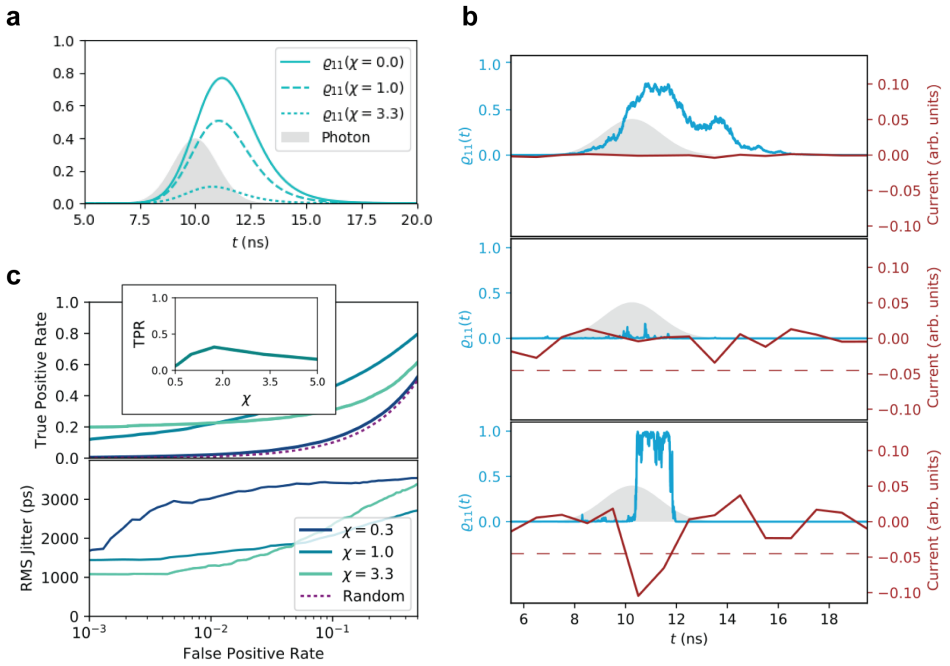

FIG. 3. Detection events and performance for Configuration 1. **a**, The averaged population dynamics for Configuration 1 with amplification strengths $\chi = 0$, $\chi = 1.0\text{ns}^{-1/2}$, and $\chi = 3.0\text{ns}^{-1/2}$. The instantaneous current is proportional to $\chi^2\rho_{11}$. **b**, Sample trajectories and current outputs for $\chi = 0.333\text{ns}^{-1/2}$ (top panel) and $\chi = 3.33\text{ns}^{-1/2}$ (bottom two panels). The horizontal dashed lines are examples of current thresholds used to calculate the ROC curves. **c**, ROC curve and jitter vs. false positive rate, for several amplification strengths obtained by computing each for varying current thresholds for detection. The dashed line is the result for "detectors" that simply record random hits at varying rates, giving equal true positive and false positive rates. In the inset, the efficiency for a false positive rate of 0.01 is plotted as a function of χ; optimal detection efficiency is obtained for intermediate amplification strength for a modest rate of false positives and strong amplification strength for minimal false positives. Stronger coupling also reduces jitter, which increases with the false positive rate.

many trajectories. Figure 3c shows the Receiver Operating Characteristics (ROC) curve obtained from simulating 1000 trajectories with a photon and 1000 trajectories without a photon, for each value of χ. The true positive rate (TPR) corresponds to the fraction of trajectories when the detector output exceeds a pre-defined threshold in the presence of a photon in the field, while the false positive rate (FPR) is when the detector output exceeds the threshold without a photon being incident on the detector. Each point on the ROC curve is for a different value of the threshold, which decreases from left to right. For large thresholds, both the TPR and the FPR are low, while for low threshold both the TPR and the FPR are high. We find a clear tradeoff between TPR and FPR regardless of the threshold used.

We also show in the inset of Fig. 3c the efficiency as a function of the amplification strength χ for a fixed FPR of 0.01. As might be anticipated from the average dynamics, the efficiency is maximized for intermediate amplification strength: too weak and the signal cannot be reliably separated from the noise, too strong and excitation is suppressed. Calculation of the RMS jitter (Fig. 3c) reveals no tradeoff with dark counts: a low FPR is associated with low jitter. Unfortunately this occurs when the TPR (efficiency) is low. At the higher efficiency levels, where intermediate coupling maximizes efficiency, we find that the same intermediate coupling also gives the lowest jitter.

Ultimately, we find that directly amplifying the optical excitation interferes with the excitation itself, creating a tradeoff between increasing the signal-to-noise ratio and avoiding amplification-induced decoherence. See also Ref. [26] for a similar analysis in a different physical context.

B. Configuration 2

In the case where the excited state decays to a dark state (Fig. 2b), the matrix equations become

$$\begin{aligned}
\dot{\rho}_{01} &= -i\omega_{01}\rho_{01} + \gamma E(t) - \frac{\gamma^2+\Gamma^2}{2}\rho_{01}; \quad \rho_{01}(0) = 0,\\
\dot{\varrho}_{00} &= 2\gamma E(t)\rho_{01} + \gamma^2\varrho_{11}; \quad \varrho_{00}(0) = 1,\\
\dot{\varrho}_{11} &= 2\gamma E(t)\rho_{01} - (\gamma^2+\Gamma^2)\varrho_{11}; \quad \varrho_{11}(0) = 0,\\
\dot{\varrho}_{CC} &= \Gamma^2\varrho_{11}; \quad \varrho_{CC}(0) = 0,
\end{aligned}$$

with all other elements zero throughout. Γ^2 is the incoherent decay rate from $|1\rangle$ to $|C\rangle$. We note that the amplification strength appears nowhere in these equations;

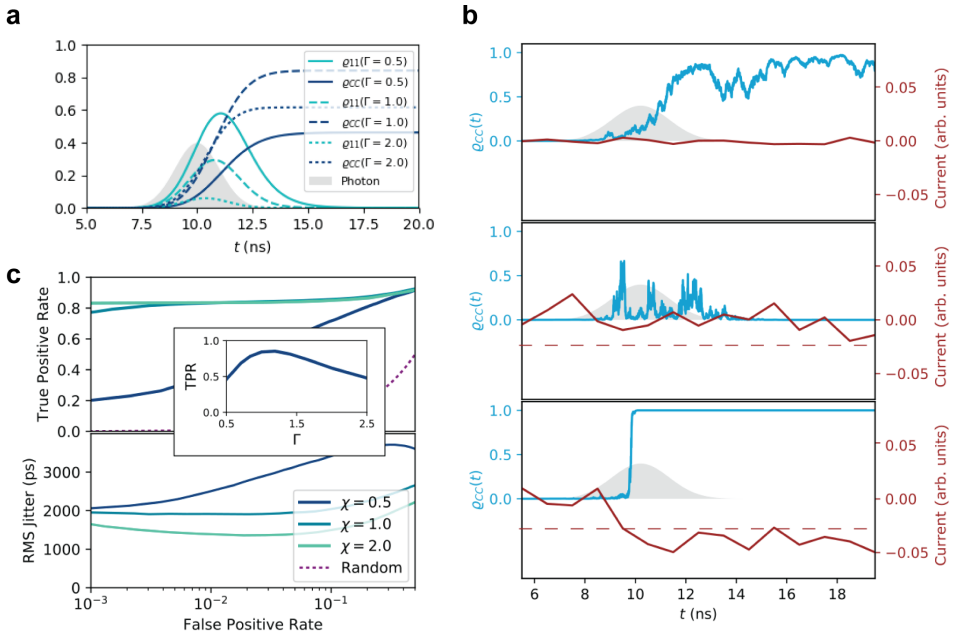

FIG. 4. Detection events and performance for Configuration 2. **a**, Average population dynamics for different values of the incoherent transfer rate Γ^2. **b**, Sample trajectories and detector output for $\chi = 0.5\text{ns}^{-1/2}$ (top panel) and for $\chi = 2.0\text{ns}^{-1/2}$ (bottom two panels) where the photon is not absorbed and when the photon induces an excitation. The horizontal dashed lines are examples of current thresholds used to calculate the ROC curves. **c**, ROC curve and jitter vs. false positive rate for several amplification strengths. Very high detection efficiency is obtained for strong amplification at essentially no cost in terms of dark count rate or jitter. The efficiency is plotted against the parameter of relaxation into the dark state Γ (inset). There is a clear maximum; faster transfer collects excitation more efficiently but inhibits the excitation process.

since the transfer from 1 to C is already fully incoherent, no decoherence due to amplification occurs. Thus, in contrast to Configuration 1, the average dynamics exhibit no influence from amplification strength and backaction. Instead, the coupling to the decay state introduces decoherence in a similar fashion as the amplification in Configuration 1. As such, it produces a similar tradeoff: there is an optimal value for the decay rate into this state. As seen in Fig. 4a, a slow decay rate allows for high excitation probabilities but low population of the measured state, while fast decay rates convert more of the excited population into the measured-state population, but reduce the excitation probability through decoherence.

Despite the *average* dynamics being insensitive to the amplification strength, the relationship between information gain and disturbance is still affected by the details of the amplification. In Eq. (5) the normalization term applies a scalar correction to the entire density matrix; this will condition *all* density matrix elements on the prior record, resulting in a nontrivial impact on the dynamics of each record, as is clearly manifested by the the individual trajectories (Fig. 4b). The strong amplification yields currents that unambiguously signal absorption or non-absorption. Moreover, in this configuration, the long lifetime of the $|C\rangle$ state results in a persistent current when the photon has been absorbed. Interestingly, although the amplification cannot influence the average populations (and hence there is no Zeno effect according to traditional definitions [25]), the amplification does effect the variance in the populations – larger χ yields a larger variance in population statistics at a fixed time.

Again, we can summarize the influence of various parameters by aggregate performance statistics (Fig. 4c). The detection efficiencies are significantly higher than for Configuration 1; moderate amplification is sufficient to guarantee optimal efficiency with negligible dark counts and no tradeoff must be negotiated. Indeed, Fig. 4c shows that for high threshold values, the TPR exceeds 0.8 while the FPR is 0.001. Similarly, jitter is much less sensitive to the detection threshold. In contrast to Configuration 1, amplification does not adversely affect optical excitation; no tradeoff exists, and both efficiency and jitter are optimized by stronger rather than intermediate amplification.

III. AN IDEAL DETECTOR

In the above, we have taken the optical coupling, γ, to be in the regime that provides optimal excitation probability for the isolated two state system [16]. This optimum occurs due to the tradeoff between excitation rate and emission rate. However, the introduction of an amplification mechanism adds both additional decoherence and protects against emission back into the field mode. This suggests that the detector may be able to take advantage of strong optical coupling. In addition, since our results indicate that relaxation into the $|C\rangle$ state should

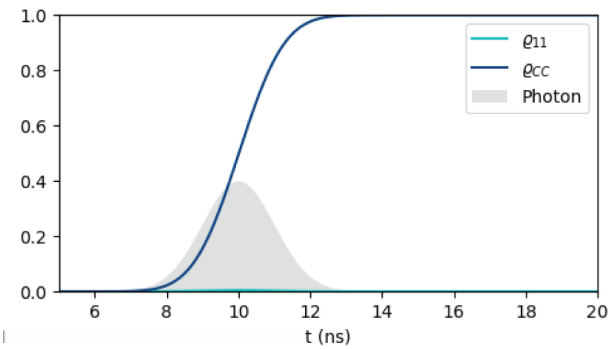

FIG. 5. The average dynamics of Configuration 2 with $\gamma^2 = \Gamma^2 = 0.1\text{ps}^{-1}$. Strong optical coupling means that excitation occurs rapidly compared to the pulse duration, and a matched rate of incoherent transfer converts excited state population to dark state population as soon as the former develops. Consequently, regardless of the strength of the quantum measurement, the measured state $|C\rangle$ attains 100% probability and the excited state $|1\rangle$ is nearly unoccupied throughout.

occur at a similar rate as the excitation, increasing the optical coupling means that the relaxation rate ought to be increased as well, further enhancing decoherence and providing protection against emission. Indeed, we find that, in contrast to the un-monitored system, the optimal optical coupling is arbitrarily high; the detector can actually achieve near perfect efficiency if both $\gamma^2 \gg 1/\sigma$ and $\gamma = \Gamma$, as shown in Fig. 5. Essentially, the pulse is absorbed as quickly as possible and the resulting excited state population is shunted to the dark state as soon as it develops, preventing re-emission. Additionally, the amplification can be made arbitrarily strong, since the coherent field-matter interaction is decoupled from its backaction by the incoherent decay process, so that dark counts can be essentially eliminated. Performing 50,000 simulations with and without a photon using $\gamma^2 = \Gamma^2 = 0.1\text{ps}^{-1}$, we find that a wide range of thresholds yield 50,000 hits, 0 dark counts, and 1.05ns of jitter, where 1.0ns jitter is the lower limit set by the wavepacket width, σ. Furthermore, almost perfect detection is possible for a wide range of single-photon pulse widths – *e.g.,* for the value $\gamma^2 = \Gamma^2 = 0.1\text{ps}^{-1}$, such ideal performance holds for pulses as short as 100ps (see Appendix for additional trajectories). For shorter pulses, efficiency is reduced (Fig. 5), as absorption no longer occurs rapidly enough to collect the entire pulse.

This demonstrates that tradeoffs in photodetection can be circumvented through detector design, and that an ideal detector is in principle possible.

IV. DISCUSSION

At the most general level, the two models discussed here represent all detectors of the kind presented in Fig. 1. Configurations that are complicated by adding intermediate states that are coherently coupled to the absorbing system and the amplification process will exhibit qualitatively similar behavior to Configuration 1; the coherent nature of the couplings will ensure that amplification backaction will be propagated back to the absorbing system, limiting performance in the fashion shown for Configuration 1, as well as exposing all states to the impact of spontaneous emission. For Configuration 2, additional states in the relaxation pathway will not impact the absorption process since the absorbing system will be insulated from the effects of any amplification dynamics after the first incoherent decay. Furthermore, provided all final states are amplified and monitored, multiple decay states and/or extended decay pathways will not qualitatively alter the results. However, for any configuration, the presence of decay processes to unmonitored states (*e.g.,* additional spontaneous emission back to the ground state) will obviously and straightforwardly limit performance.

The lesson then from studying these systems is that any system where the amplification acts on the absorbing subsystem, directly or via a coherent chain, will necessarily face a compromised absorption process, sharply limiting the performance, and answering the question of whether preserving coherence up to amplification yields any improvements. Additionally, if irreversible decay occurs from the optically active subsystem to an optically inactive subsystem, as in Configuration 2, one can decouple the amplification process from the light-matter interaction and achieve performance arbitrarily close to ideal. However, in this case one has to engineer the rate of the first relaxation process to match to the optical coupling strength, which itself must be high compared to the inverse of the pulse durations one desires to detect.

Finally, we believe that current high-performance single-photon detectors are operating in regimes that are close to the one described by Configuration 2. Both avalanche photodiodes and superconducting detectors rely on rapid incoherent decay from an optically excited coherent state to optically inert intermediate states before amplification. Our results clearly show why these types of detectors offer the superior performance they are known for, and suggest that in principle this class of detectors may be tuned to operate perfectly. Moreover, recent proposals and prototypes of single photon detectors in the microwave regime operate using internal detector structure that is very similar to Configuration 2 [27, 28]. Thus the fundamental tradeoffs and limiting mechanisms we have identified can provide design principles for guiding future efforts to engineer new photodetector types regardless of the underlying physical mechanisms.

ACKNOWLEDGMENTS

Work supported by the DARPA DETECT program. Sandia National Laboratories is a multimission laboratory managed and operated by National Technology and

Engineering Solutions of Sandia, LLC., a wholly owned subsidiary of Honeywell International, Inc., for the U.S. Department of Energy's National Nuclear Security Administration under contract DE-NA-0003525. We thank Baptiste Royer for informing us of recent single photon detection work in the microwave regime.

[1] R. J. Glauber, Phys. Rev. Lett. **10**, 84 (1963).
[2] P. L. Kelley and W. H. Kleiner, Phys. Rev. **136**, A316 (1964).
[3] M. O. Scully and W. E. Lamb, Phys. Rev. **179**, 368 (1969).
[4] M. Ueda, Phys. Rev. A **41**, 3875 (1990).
[5] L. Mandel and E. Wolf, *Optical Coherence and Quantum Optics* (Cambridge University Press, 1995).
[6] J. C. Bienfang, A. J. Gross, A. Mink, B. J. Hershman, A. Nakassis, X. Tang, R. Lu, D. H. Su, C. W. Clark, C. J. Williams, E. W. Hagley, and J. Wen, Optics Express **12**, 2011 (2004).
[7] M. E. Woodson, M. Ren, S. J. Maddox, Y. Chen, S. R. Bank, and J. C. Campbell, Applied Physics Letters **108**, 081102 (2016).
[8] W. H. P. Pernice, C. Schuck, O. Minaeva, M. Li, G. N. Goltsman, A. V. Sergienko, and H. X. Tang, Nature **3**, 1325 (2012).
[9] F. Marsili, F. Bellei, F. Najafi, A. E. Dane, E. A. Dauler, R. J. Molnar, and K. K. Berggren, Nano. Lett. **12**, 4799 (2012).
[10] F. Marsili, V. B. Verma, J. A. Stern, S. Harrington, A. E. Lita, T. Gerrits, I. Vayshenker, B. Baek, M. D. Shaw, R. P. Mirin, and S. W. Nam, Nature Photonics **7**, 210 (2013).
[11] M. D. Eisaman, J. Fan, A. Migdall, and S. V. Polyakov, Review of Scientific Instruments **82**, 071101 (2011).
[12] R. H. Hadfield, Nat. Photon. **3**, 696 (2009).
[13] H.-P. Breuer and F. Petruccione, *The theory of open quantum systems* (Oxford University Press, 2002).
[14] B. Q. Baragiola, R. L. Cook, A. M. Branczyk, and J. Combes, Phys. Rev. A **86**, 013811 (2012).
[15] K. M. Gheri, K. Ellinger, T. Pellizzari, and P. Zoller, Fortschritte der Physik **46**, 401 (1998).
[16] Y. Wang, J. Minář, L. Sheridan, and V. Scarani, Phys. Rev. A **83**, 063842 (2011).
[17] C. M. Caves and G. J. Milburn, Phys. Rev. A **36**, 5543 (1987).
[18] J. D. Cresser, S. M. Barnett, J. Jeffers, and D. T. Pegg, Optics Communications **264**, 352 (2006).
[19] K. Jacobs and D. A. Steck, Contemp. Phys. **47**, 279 (2006).
[20] C. M. Caves, Phys. Rev. **26**, 1817 (1982).
[21] A. A. Clerk, S. M. Girvin, F. Marquardt, and R. J. Schoelkopf, Rev. Mod. Phys. **82**, 1155 (2010).
[22] H. M. Wiseman and G. J. Milburn, *Quantum measurement and control* (Cambridge University Press, 2009).
[23] A. Rößler, SIAM Journal on Numerical Analysis **48**, 922 (2010).
[24] B. Misra and E. C. G. Sudarshan, J. Math. Phys. **18**, 756 (1977).
[25] P. Facchi and S. Pascazio, Prog. Optics **42**, 147 (2001).
[26] F. Helmer, M. Mariantoni, E. Solano, and F. Marquardt, Phys. Rev. A **79**, 052115 (2009).
[27] Y. F. Chen, D. Hover, S. Sendelbach, L. Maurer, S. T. Merkel, E. J. Pritchett, F. K. Wilhelm, and R. McDermott, Phys. Rev. Lett. **107**, 217401 (2011).
[28] K. Inomata, Z. Lin, K. Koshino, W. D. Oliver, J.-S. Tsai, T. Yamamoto, and Y. Nakamura, Nature **7**, ncomms12303 (2016).
[29] X. Zhou, T. Zifer, B. M. Wong, K. L. Krafcik, F. Leonard, and A. L. Vance, Nano Letters **9**, 1028 (2009).
[30] H.-S. Goan, G. J. Milburn, H. M. Wiseman, and H. B. Sun, Phys. Rev. B **63**, 125326 (2001).

APPENDIX I: EXAMPLE DERIVATION OF MASTER EQUATION FROM PHYSICAL SYSTEM

In this section we derive a stochastic master equation representing a concrete physical system to illustrate the general formalism presented in the main text. Fig. 6 shows a schematic of the "device" for which we will write a dynamical model. It consists of a photoactive molecule positioned near a short-channel ((*e.g.,* 10nm) carbon nanotube (CNT) connected to leads. There are three relevant states in the molecule: the ground state $|0\rangle$, an excited state $|1\rangle$ optically connected to the ground state, and an optically dark state $|C\rangle$ that represents the state of the molecule after photon absorption, such as can arise from photoisomerization. The static dipole of the molecule is different (in magnitude and direction) in states $|1\rangle$ and $|C\rangle$ and this change induces a change in the electrostatic potential of the CNT and as a result, the current across it. Such systems have been previously studied experimentally [29].

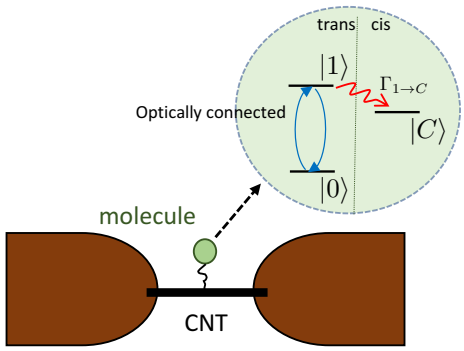

FIG. 6. A schematic of a molecular photodetection device. Photons are absorbed by the molecular system (internal structure shown), and the detection event is amplified by electronic transport in the carbon nanotube. A quantum measurement master equation for the dynamics of this device is developed in this section.

In order to develop a model for this device, we will approximate the transport of electrons across the nanotube as a tunneling process, which is justified by the short channel length. The tunnel barrier is set by the energy levels in the nanotube. Given this simplification, we can model the system using a Hamiltonian $H = H_f + H_{f-m} + H_m + H_{m-CNT} + H_{CNT}$, where H_f, H_m and H_{CNT} are the bare electromagnetic (EM) field, molecule and CNT Hamiltonians, respectively. H_{f-m} is the field-molecular interaction, and H_{m-CNT} is the molecule-CNT interaction. Explicitly, these Hamiltonians are:

$$\begin{aligned} H_m &= \hbar\omega_0 |0\rangle\langle 0| + \hbar\omega_1 |1\rangle\langle 1| + \hbar\omega_C |C\rangle\langle C| \\ H_{CNT} &= \sum_k (\hbar\omega_k^L a_{Lk}^\dagger a_{Lk} + \hbar\omega_k^R a_{Rk}^\dagger a_{Rk} \\ &\quad + \sum_{k,q} (T_{kq} a_{Lk}^\dagger a_{Rq} + T_{qk}^* a_{Rq}^\dagger a_{Lk}) \\ H_{m-CNT} &= \sum_{k,q} |C\rangle\langle C| (\chi_{kq} a_{Lk}^\dagger a_{Rq} + \chi_{qk}^* a_{Rq}^\dagger a_{Lk}). \end{aligned} \quad (6)$$

We will leave H_f and H_{f-m} unspecified at this point. In the above, $\hbar\omega_0, \hbar\omega_1, \hbar\omega_C$ are the energies of the respective states of the molecule. $\hbar\omega_k^L$ and $\hbar\omega_k^R$ are the energies of left and right reservoir/lead states at wavenumber k, and a_{Lk}, a_{Rk} are (fermionic) annihilation operators for these states. T_{kq} is the tunneling matrix element between states k and q in the left and right reservoir, and χ_{kq} is the perturbation to this element due to the molecule being in state $|C\rangle$. Note that this effectively means that the tunneling amplitude goes from T_{kq} to $T_{kq} + \chi_{kq}$ when the molecule is in the $|C\rangle$ state.

In addition to these coherent dynamics, the different conformational states $|1\rangle$ and $|C\rangle$ are connected by an incoherent rate $\Gamma^2_{1\to C}$ (and we assume the backward transition rate $\Gamma^2_{C\to 1}$ is negligible).

This model for the CNT and molecule-CNT interaction are similar to the model used for quantum point contact based measurement in Ref. [30]. Following that reference, we can now derive a master equation describing the dynamics of the molecule and light degrees of freedom only by integrating out the continuum of reservoir states:

$$\begin{aligned} \dot{\varrho}(t) &= -\tfrac{i}{\hbar}[H_f + H_{f-m} + H_m, \varrho] + \Gamma_{1\to C}\mathcal{D}[|C\rangle\langle 1|]\varrho(t) \\ &\quad + \mathcal{D}[\mathcal{T}_+ + \mathcal{X}_+ |C\rangle\langle C|]\varrho(t) \\ &\quad + \mathcal{D}[\mathcal{T}_-^* + \mathcal{X}_-^* |C\rangle\langle C|]\varrho(t) \\ &\equiv -\tfrac{i}{\hbar}[H_f + H_{f-m} + H_m, \varrho] + \mathcal{L}_t\varrho \end{aligned} \quad (7)$$

where ϱ is the density matrix for the molecular and field degrees of freedom only. In this equation, $\mathcal{D}$ is a superoperator defined as:

$$\mathcal{D}[A]\rho = A\rho A^\dagger - \tfrac{1}{2} A^\dagger A\rho - \tfrac{1}{2} \rho A^\dagger A \quad (8)$$

Before specifying the coefficients $\mathcal{T}_\pm$ and $\mathcal{X}_\pm$ we repeat from Ref. [30] all the assumptions that go into deriving this master equation:

1. The left and right reservoirs/leads are thermal equilibrium free electron baths.
2. Weak coupling between molecule and CNT, which effectively means that we can restrict ourselves to a second order expansion in χ_{kq}, T_{kq}.
3. The transport through the channel (CNT/QPC) is in the tunnel junction limit – *i.e.,* low transmmitivity.

4. The initial state of the molecule and CNT are uncorrelated/factorizable.

5. Fast relaxation of the reservoirs – *i.e.,* the degrees of freedom in the reservoirs relax to equilibrium much faster than any system timescales.

6. Markovian approximation of the reservoir.

7. If eV is the external bias applied across the transport channel, and μ_L, μ_R are the chemical potentials in the left and right reservoirs (*i.e.,* $eV = \mu_L - \mu_R$), then $|eV|, k_B T \ll \mu_{L(R)}$.

8. Energy independent tunneling amplitudes and density of states over the bandwidth $\max(|eV|, k_b T)$.

Under these approximations, the dynamics of the system is described by the above master equation, with the coefficient determined by

$$\begin{aligned} |\mathcal{T}_\pm|^2 &= \tfrac{2\pi e}{\hbar}\, |T_{00}|^2 g_L g_R V_\pm \\ |\mathcal{T}_\pm + \mathcal{X}_\pm|^2 &= \tfrac{2\pi e}{\hbar}\, |T_{00} + \chi_{00}|^2 g_L g_R V_\pm, \end{aligned} \tag{9}$$

where T_{00}, χ_{00} are the energy-independent tunneling amplitudes near the average chemical potential, g_L, g_R are the energy-independent density of states in the left and right reservoirs, respectively. The finite temperature effective external bias is:

$$eV_\pm \equiv \frac{\pm eV}{1 - \exp\left(\frac{\mp eV}{k_B T}\right)} \tag{10}$$

At first approximation, we can work in the limit of low temperature and ignore the thermally activated current in the reverse direction, and set $V_- = 0$, which will effectively remove the third term in Eq. (7).

Eq. (7) can be interpreted as a measurement master equation giving the averaged dynamics when the population in the state $|C\rangle$ is continuously monitored [30]. Conditioned dynamics, based on particular values of the current can also be derived from the corresponding stochastic master equation [22]:

$$\begin{aligned} d\varrho(t) = &- \tfrac{i}{\hbar}\,[H_f + H_{f-m} + H_m, \varrho]dt + \mathcal{L}_t \varrho dt \\ &+ \mathcal{H}[\mathcal{T}_+ + \mathcal{X}_+ \,|C\rangle\langle C|]\varrho(t) dW_+(t) \\ &+ \mathcal{H}[\mathcal{T}_-^* + \mathcal{X}_-^* \,|C\rangle\langle C|]\varrho(t) dW_-(t), \end{aligned}$$

where $\mathcal{H}[A]\varrho \equiv A\varrho + \varrho A^\dagger - \left\langle A + A^\dagger \right\rangle_\varrho \varrho$, and $dW_+(t)$ and $dW_-(t)$ are Wiener increments. Increments in the forward and reverse current consistent with this evolution are given by:

$$\begin{aligned} dI_+(t) &= \langle \mathcal{T}_+ + \mathcal{X}_+ \,|C\rangle\langle C| \rangle_\varrho \, dt + dW_+(t), \\ dI_-(t) &= \left\langle \mathcal{T}_-^* + \mathcal{X}_-^* \,|C\rangle\langle C| \right\rangle_\varrho dt + dW_-(t), \end{aligned}$$

APPENDIX II: QUANTUM TRAJECTORIES FOR IDEAL DETECTOR

In this section we present additional trajectories for the "ideal photodetector" for different values of the photon wavepacket width. Figure 7 shows that for pulse widths ranging from 100ps to 1ns the collection efficiency is 100%.

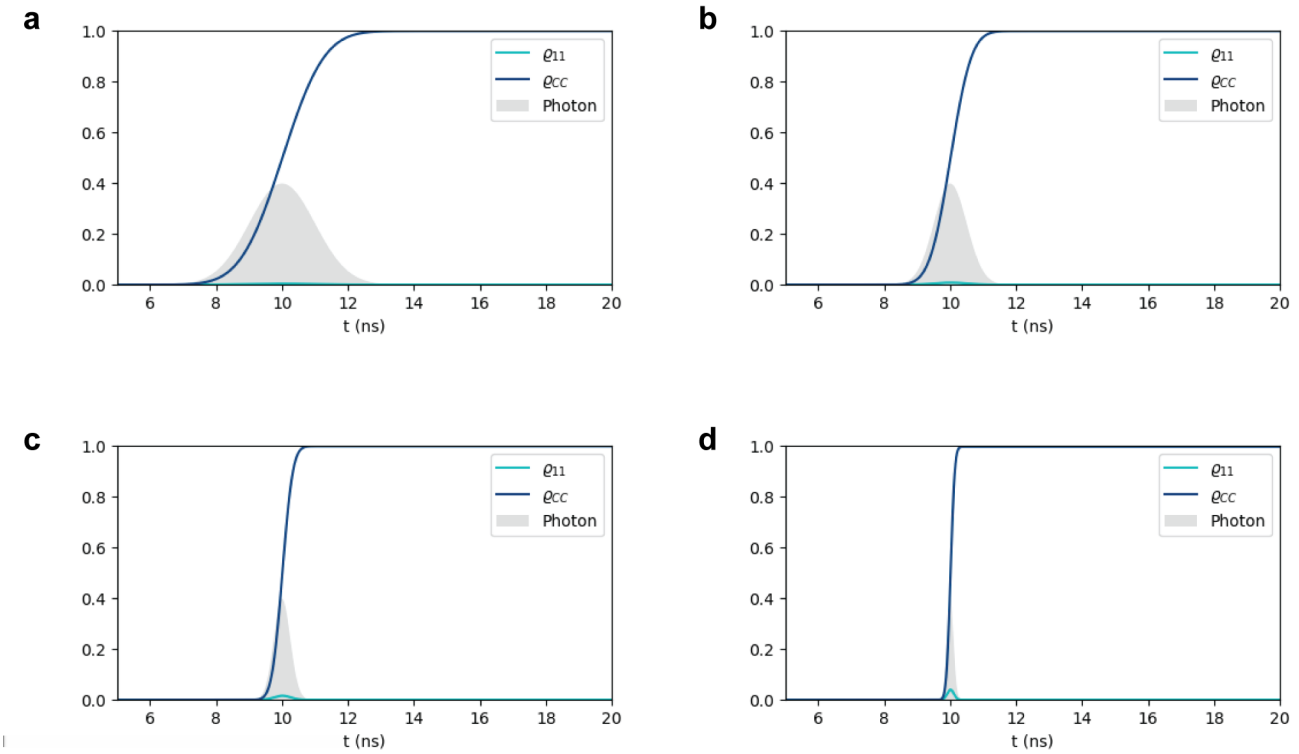

FIG. 7. The average dynamics of the three state system with $\gamma^2 = \Gamma^2 = 0.1\text{ps}^{-1}$ for wavepackets of widths **a**, 1ns, **b**, 500ps, **c**, 250ps, and **d**, 100ps. We see that in all cases the photon is collected 100% of the time.